

Evolutionary reinforcement learning of dynamical large deviations

Stephen Whitelam^{1,*}, Daniel Jacobson², and Isaac Tamblyn^{3,4}

¹*Molecular Foundry, Lawrence Berkeley National Laboratory,
1 Cyclotron Road, Berkeley, CA 94720, USA*

²*Division of Chemistry and Chemical Engineering,
California Institute of Technology,
Pasadena, California 91125, USA*

³*University of Ottawa* & ⁴*National Research Council of Canada,
Ottawa, ON, Canada*

We show how to calculate dynamical large deviations using evolutionary reinforcement learning. An agent, a stochastic model, propagates a continuous-time Monte Carlo trajectory, and receives a reward conditioned upon the values of certain path-extensive quantities. Evolution produces progressively fitter agents, allowing the calculation of a piece of a large-deviation rate function for a particular model and path-extensive quantity. For models with small state spaces the evolutionary process acts directly on rates, and for models with large state spaces the process acts on the weights of a neural network that parameterizes the model's rates. The present approach shows how path-extensive physics problems can be considered within a framework widely used in machine learning.

Introduction— Machine learning has begun to provide the physics community with methods that complement the traditional ones of physical insight and manipulation of equations. Many-parameter ansätze, sometimes encoded in the form of neural networks, can learn connections between physical properties (such as the positions of atoms and a system's internal energy) and detect phase transitions, without drawing upon an underlying physical model [1–14]. Reinforcement learning (RL) is a branch of machine learning concerned with learning a set of actions, through interactions with an environment, so as to maximize a numerical reward [15]. It has a close connection to ideas of stochastic control enacted by variational or adaptive algorithms [16–21]. A recent success of reinforcement learning is the playing of computer games [22–39]. Here we show that reinforcement learning can also be used to propagate trajectories of a stochastic dynamics conditioned upon potentially very rare values of a path-extensive observable. Doing so allows the calculation of dynamical large deviations, which are of fundamental importance, being to dynamical quantities what free energies are to static ones [40–43].

Calculating large deviations is a challenging problem for which only a few numerical methods have been developed [16, 18, 19, 40, 41, 44–47]. The RL procedure we describe, equivalent to dynamic importance sampling in continuous time [40, 42, 48–55], is conceptually and technically simple, and does not require insight into the models under study or access to the formal results of large-deviation theory. It therefore offers an alternative to existing approaches, and provides an example of one of the potentially large number of applications of reinforcement learning in physics.

Large deviations by change of dynamics— To set the large-deviations problem in a form amenable to reinforce-

ment learning, consider a continuous-time Monte Carlo dynamics on a set of discrete states, with W_{xy} the rate for passing between states x and y , and $R_x = \sum_{y \neq x} W_{xy}$ the escape rate from x [56]. This dynamics generates a trajectory $\omega = x_0 \rightarrow x_1 \rightarrow \dots \rightarrow x_{N(\omega)}$ consisting of $N(\omega)$ jumps $x_n \rightarrow x_{n+1}$ and associated jump times Δt_n . In the language of reinforcement learning, W_{xy} is a policy (often denoted π) that stochastically selects a new state and a jump time given a current state.

Stochastic trajectories can be characterized by path-extensive observables $A = aT$, with

$$a = T^{-1} \sum_{n=0}^{N-1} \alpha_{x_n x_{n+1}}. \quad (1)$$

Here α_{xy} is the change of the observable upon moving between x and y . This type of observable describes many physically important quantities, including work, entropy production, and non-decreasing counting observables [41, 57–60]. Let the typical value of a be a_0 , the limiting value of (1) for a long trajectory of the model W_{xy} . Finite-time fluctuations $a \neq a_0$ occur with a probability controlled by the distribution $\rho_T(A)$, taken over all trajectories of length T , which for large T often adopts the large-deviation form [40, 42]

$$\rho_T(A) \approx e^{-TJ(a)}. \quad (2)$$

$J(a)$ is the large-deviation rate function, which quantifies the likelihood of observing atypical values of a [40, 42]. Calculation of $J(a)$ far from a_0 using only the original model is not feasible, precisely because observing $a \neq a_0$ is unlikely. Instead, we can consider a new stochastic model, which we call the reference model, whose purpose is to allow reconstruction of $J(a)$ potentially far from a_0 [16, 54]. Let the rates of the reference model be \tilde{W}_{xy} and $\tilde{R}_x = \sum_{y \neq x} \tilde{W}_{xy}$, and let the limiting value of (1) for a long reference-model trajectory be \tilde{a}_0 . Then an upper

* swhitelam@lbl.gov

bound on $J(a)$ at $a = \tilde{a}_0$ is given by the value of

$$J_0 = -T^{-1} \sum_{n=0}^{N-1} q_{x_n x_{n+1}} \quad (3)$$

for a long reference-model trajectory, where

$$q_{x_n x_{n+1}} = \ln \frac{W_{x_n x_{n+1}}}{\tilde{W}_{x_n x_{n+1}}} - \tilde{\Delta} t_n (R_{x_n} - \tilde{R}_{x_n}). \quad (4)$$

Here $\tilde{\Delta} t_n = -\ln \eta / \tilde{R}_{x_n}$ is the jump time of the reference model, and η is a random number uniformly distributed on $(0, 1]$. Eq. (3) follows from straightforward algebra (see Section S1). It can be motivated by noting that the probability of a jump $x \rightarrow y$ in time $\tilde{\Delta} t$ occurs in the reference model with probability $\tilde{W}_{xy} e^{-\tilde{R}_x \tilde{\Delta} t}$, and in the original model with probability $W_{xy} e^{-R_x \tilde{\Delta} t}$; Eq. (3) is the sum over a trajectory of the log-ratio of such terms.

Our aim is to use evolutionary reinforcement learning to find a reference model (a new policy) \tilde{W}_{xy} that produces particular values of (1), and, given this, minimizes (3). Formulated in this way this is an extreme example of reinforcement learning in which there is no instantaneous reward, only an overall reward (or return) associated with the entire trajectory [15]. Given that we possess a constraint on a and work in continuous time, this problem also falls outside the Markov decision process framework [61, 62].

Large deviations via evolutionary reinforcement learning—As proof of principle we consider the example of entropy production in the 4-state model [63] of Ref. [64]. The model's rates do not satisfy detailed balance, and so it produces nonzero entropy on average. The dynamical observable a is (1) with $\alpha_{xy} = \ln(p_{xy}/p_{yx})$, where $p_{xy} = W_{xy}/R_x$. In Fig. 1(a) we depict the model (the middle picture), with states x numbered clockwise from 1 in the top left. Red and blue links denote connections $x \rightarrow y$ with positive and negative entropy production, respectively, and the thickness of the links is proportional to the rate associated with the connection. The model's state space is small enough that the master operator can be solved by diagonalization [40], yielding the exact rate function $J(a)$, shown as a black dashed line in Fig. 1(b).

We perform evolutionary reinforcement learning by mutating the rates \tilde{W}_{xy} of a set of reference models until desired values of (1) and (3) are achieved (see Section S2). Some of the models produced in this way are shown in Fig. 1(a), and the associated rate-function values are shown in panel (b). All points (\tilde{a}_0, J_0) derived from the reference models lie on the exact rate function of the original model (if we did not possess the exact answer we could verify, by measuring the fluctuations of the reference models, that this is the case [55]), indicating that each reference model's typical dynamics is equivalent to the conditioned rare dynamics of the original model. Some of the reference models so obtained are shown in panel (a) and in the right-bottom inset of

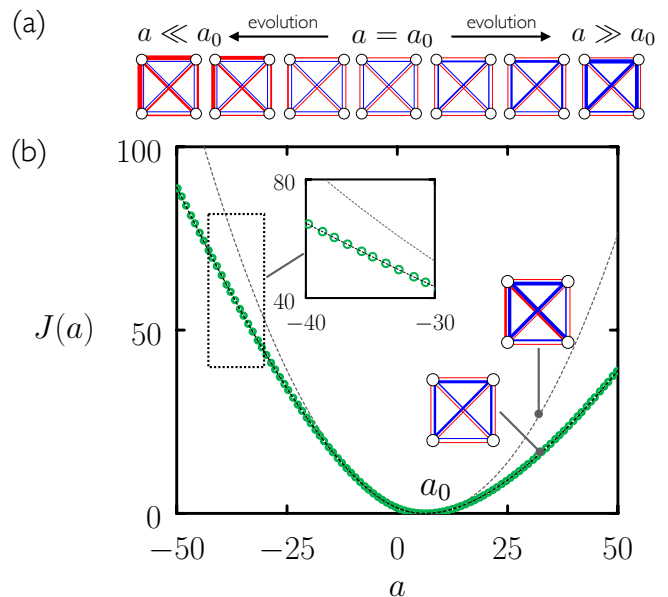


FIG. 1. (a) Evolutionary reinforcement learning can produce versions of the 4-state model of Ref. [64] whose typical dynamics are exactly equivalent to the rare dynamics of the original model (center) conditioned on values of entropy production a . (b) From these we can calculate the corresponding large-deviation rate function, $J(a)$. The black dashed line is the exact answer, obtained by matrix diagonalization [40, 42], and the gray dashed line is the universal current bound [64, 65]. The green points describe a bound resulting from a set of models generated by evolutionary reinforcement learning; this bound is exact. Each green point is calculated using a single trajectory of a stochastic model produced by the evolutionary process. Inset left: enlargement of the boxed area. Inset right: we contrast one model (lower) produced by evolution (see panel (a)) with a second model (upper) that produces the same typical value of a but whose rates are uniformly scaled versions of the original model.

panel (b). The gray dashed line is the universal current rate-function bound [64, 65]. This bound measures, for given a , the probability with which typical trajectories of a reference model whose rates are uniformly rescaled versions of the original model (right-top inset) would have been generated by the original model. Such trajectories are much less likely than are trajectories of the models identified by evolution.

A neural-network ansatz for models with large state spaces—Thus evolutionary reinforcement learning using 12 trainable parameters (the 12 rates of the reference model) has permitted accurate computation of probabilities exponentially small in the trajectory length T . However, direct application of rate-based evolution is impractical for models with a large number of rates, necessitating a more efficient representation of those rates [15, 16]. One way to do this is to encode the rates of the reference model in the form of a neural network. As an illustration of this procedure we consider the one-dimensional Fredrickson-Andersen (FA) model with periodic bound-

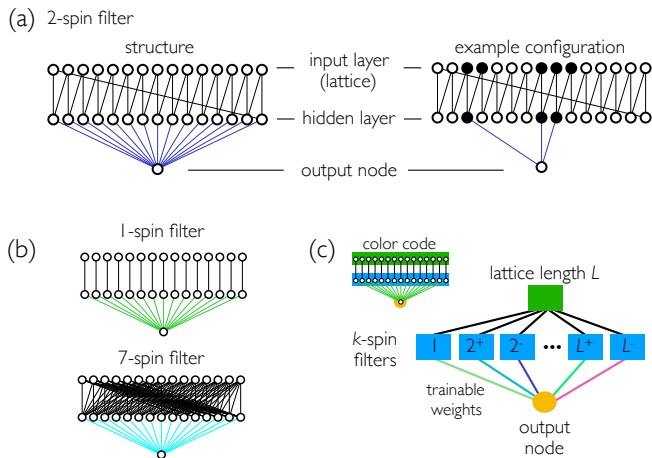


FIG. 2. Sketch of the neural-network reference-model ansatz used to compute the dynamical large deviations of the FA lattice model. (a) The building block of the network is a k^α -spin “filter”, whose hidden nodes activate when the k consecutive spins to which they are attached are all of type $\alpha = \pm$ (periodic boundaries account for the diagonal line between input and hidden layers). Here we show a 2^+ -spin filter applied to a lattice of $L = 15$ sites; shown right is an example configuration. The output of the filter is the number of hidden nodes that are on (here 3) multiplied by the weights denoted by the blue lines. (b) Structure of a 1-spin filter and a 7-spin filter (lattice size $L = 15$). (c) The complete network contains a single hidden layer of $2L$ filters, with $2L$ trainable parameters (the colored lines). The network output is the function f displayed in (6).

ary conditions [67]. This is a lattice model with dynamical rules that give rise to slow relaxation and complex space-time behavior [68]. On each site i of a lattice of length L lives a spin S_i , which can be up (+1) or down (-1). Up spins (resp. down spins) flip down (resp. up) with rate $1 - c$ (resp. c) if at least one of their neighboring spins is up; if not, then they cannot flip. We take the dynamical observable a to be the number of configuration changes per unit time, $\alpha_{xy} = 1$, often called activity [41, 69]. To determine the large-deviation rate function $J(a)$ for activity we chose a reference-model parameterization

$$\tilde{W}_{xy} = W_{xy} e^{w_0} e^{f_y - f_x}. \quad (5)$$

Here w_0 is a parameter that effectively speeds up or slows down the clock [55], and f_x is the value in state x of the neural network sketched in Fig. 2. This network is inspired by the convolutional neural networks used to recognize images [70, 71], and consists of a set of spin “filters” that scan the lattice for specified spin patterns. Here we consider filters called k^α , each having L hidden nodes; the output of a node is 1 if the k consecutive spins to which it is attached are all in state α , and is zero otherwise (i.e. the activation function is a step function). The network has one hidden layer. The weights connecting the input layer (the lattice) to the hidden layer are unity,

and the weights connecting the hidden layer to the output node are denoted w_k^\pm ; these are the trainable parameters of the network. All weights within a filter have the same value, a constraint suggested by the translational invariance of the model. The output of the network is

$$f_x = w_1 g_1(\mathbf{S}_x) + \sum_{k=2}^K \sum_{\alpha=\pm 1} w_k^\alpha g_k^\alpha(\mathbf{S}_x), \quad (6)$$

where \mathbf{S}_x is the configuration of the lattice in state x , and $g_k^\alpha(\cdot)$ returns the number of active hidden nodes in the filter k^α [see Fig. 2(a)]. The reference model contains $2K$ trainable parameters: w_0, w_1 (only one type of 1-spin filter is necessary), and $w_2^\pm, w_3^\pm, \dots, w_K^\pm$; $K = L$ when all filter types are used.

The form of (6) is similar to the multi-parameter auxiliary potential of Ref. [18], used to improve the convergence of the cloning method [44] in order to calculate the large-deviation function of the FA model. The present approach is different, however, in that the calculation is done using direct simulations of a reference model whose parameters are determined by an evolutionary process (rather than using rare-event algorithms such as cloning or transition-path sampling [72]), and results in the calculation of $J(a)$ directly (rather than its Legendre transform).

To test the method we considered the FA model with $c = 0.3$ and $L = 15$, the latter value small enough that the exact $J(a)$ can be determined by diagonalization of the model’s rate matrix; that function is shown as a black dashed line in Fig. 3(a). We next introduce the reference model (5), and do evolutionary reinforcement learning on the weights of the network (see Section S3). In Fig. 3(a) we show results using spin filters up to order $K = 7$. Increasing K from 0 improves the quality of the bound until, for $K \gtrsim 4$, the bound becomes numerically close to the exact answer (Fig. S2). The neural network contains many fewer parameters than the model has rates (unlike in many deep-learning studies), and so we do not necessarily expect the bound to be exact. As long as it is tight enough, the exact answer can be calculated by computing a correction term [55]. Here, though, the correction term is very small, indicating that the typical dynamics of this set of reference models is statistically similar to the conditioned rare behavior of the original model. Comparison of these results with the exact result, and with the (c, λ) -bound from Ref. [55] (Fig. S2), indicates that rare trajectories of the FA model with parameter c resemble the typical trajectories of versions of the FA model with different values of the parameter c , but with slightly different tendencies to display spin domains of different lengths. These tendencies are quantified by the weights of the neural network, some of which are shown in Fig. 3(b). In panel (c) we show space-time plots of the trajectories of 5 reference models.

When applied to a model with a very large state space, whose rate-function calculation requires state-of-the-art numerical methods [47], the network shown in Fig. 2,

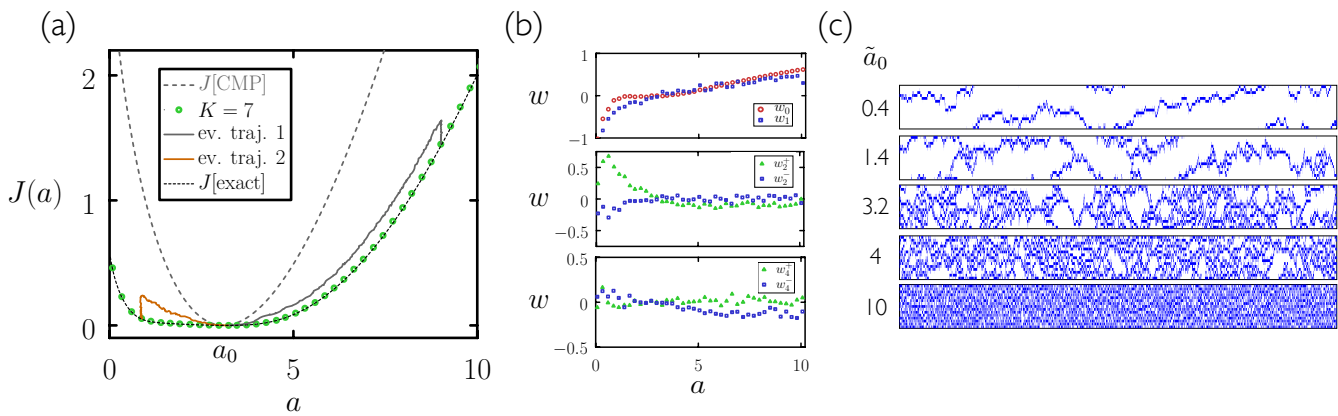


FIG. 3. (a) Evolutionary reinforcement learning using neural-network spin filters up to order $K = 7$ (green circles) reproduces the large-deviation rate function $J(a)$ for activity a in the FA model of $L = 15$ sites (black). Also shown is the CMP universal activity bound [66] (gray dashed), which results from a set of reference models whose rates are uniform multiples of those of the original model (see Section S4), and evolutionary trajectories of two neural-network reference models (gray and orange). (b) Values of some of the weights of the neural network (6) for the reference models that produce the green circles in panel (a). (c) Space (vertical) versus time (horizontal) plots for trajectories of length $T = 2 \times 10^3$ for 5 different reference models. Blue pixels indicate up-spins. The typical values of the activity for each model are shown left of the plot; the center reference model is the original model.

using $K = 5$ (10 trainable parameters) produces a bound that is inexact (Fig. S3), but close enough to the exact answer to suggest that the present approach can be used to tackle such large-scale problems. In a forthcoming paper we will address this case using a set of spin filters able to learn to identify different patterns, as opposed to the fixed-pattern filters used here.

Conclusions— We have shown that the calculation of dynamical large deviations can be done using direct simulation guided by evolutionary reinforcement learning. In previous work we showed how to calculate dynamical large deviations using a variational ansatz for rare dynamics (VARD) containing a few parameters motivated by physical insight [55]; here we show that evolutionary reinforcement learning using a multi-parameter ansatz or “VARDnet” removes the need for such insight. Evolved models allow the accurate calculation of probabilities exponentially small in the length of the path, far beyond the reach of simulations of the original model. Our approach does not rely on the formal results of large-deviation theory, making it complementary to the growing body of methods based on such results [16, 18, 19, 40, 41, 44–46]. Our results also suggest ways of addressing other physi-

cal problems. For one, the neural-network ansatz shown in Fig. 2 treats a lattice model much as a convolutional neural network treats images, and it is straightforward to imagine extending this approach to other models and higher spatial dimensions, taking the pixels of the configuration as information on which the evolutionary process can act. More generally, many physical problems involve time- or path-extensive quantities – for instance, the yield of molecular self-assembly depends on the history of the interactions of molecules – and we have shown that it is possible to generate dynamical trajectories conditioned upon rare instances of path-extensive quantities without physical insight or access to formal results.

Acknowledgments— We thank Hugo Touchette for comments. This work was performed as part of a user project at the Molecular Foundry, Lawrence Berkeley National Laboratory, supported by the Office of Science, Office of Basic Energy Sciences, of the U.S. Department of Energy under Contract No. DE-AC02-05CH11231. D.J. acknowledges support from the Department of Energy Computational Science Graduate Fellowship. I.T. performed work at the National Research Council of Canada under the auspices of the AI4D Program.

[1] J. Behler and M. Parrinello, Phys. Rev. Lett. **98**, 146401 (2007).
 [2] K. Mills, M. Spanner, and I. Tamblyn, Physical Review A **96**, 042113 (2017).
 [3] A. L. Ferguson and J. Hachmann, Molecular Systems Design & Engineering (2018).
 [4] N. Artrith, A. Urban, and G. Ceder, The Journal of Chemical Physics **148**, 241711 (2018).

[5] A. Singraber, T. Morawietz, J. Behler, and C. Dellago, Journal of Physics: Condensed Matter **30**, 254005 (2018).
 [6] C. Desgranges and J. Delhommelle, The Journal of Chemical Physics **149**, 044118 (2018).
 [7] B. Thurston and A. Ferguson, Molecular Simulation, 1 (2018).
 [8] A. Singraber, J. Behler, and C. Dellago, Journal of chemical theory and computation **15**, 1827 (2019).

- [9] K. T. Schütt, F. Arbabzadah, S. Chmiela, K. R. Müller, and A. Tkatchenko, *Nature Communications* **8**, 13890 (2017).
- [10] K. Yao, J. E. Herr, D. Toth, R. Mckintyre, and J. Parkhill, *Chem. Sci.* **9**, 2261 (2018).
- [11] K. T. Schütt, H. E. Sauceda, P.-J. Kindermans, A. Tkatchenko, and K.-R. Mller, *The Journal of Chemical Physics* **148**, 241722 (2018).
- [12] J. Carrasquilla and R. G. Melko, *Nature Physics* **13**, 431 (2017), 1605.01735.
- [13] N. Portman and I. Tamblyn, *Journal of Computational Physics* **350**, 871 (2017).
- [14] B. S. Rem, N. Käming, M. Tarnowski, L. Asteria, N. Fläschner, C. Becker, K. Sengstock, and C. Weitenberg, *Nature Physics* (2019), 10.1038/s41567-019-0554-0.
- [15] R. S. Sutton and A. G. Barto, *Reinforcement learning: An introduction* (2018).
- [16] R. Chetrite and H. Touchette, *Journal of Statistical Mechanics: Theory and Experiment* **2015**, P12001 (2015).
- [17] H. J. Kappen and H. C. Ruiz, *Journal of Statistical Physics* **162**, 1244 (2016).
- [18] T. Nemoto, R. L. Jack, and V. Lecomte, *Physical Review Letters* **118**, 115702 (2017).
- [19] G. Ferré and H. Touchette, arXiv preprint arXiv:1803.11117 (2018).
- [20] J. Han and W. E, arXiv preprint arXiv:1611.07422 (2016).
- [21] T. A. Bojesen, *Phys. Rev. E* **98**, 063303 (2018).
- [22] C. J. Watkins and P. Dayan, *Machine learning* **8**, 279 (1992).
- [23] V. Mnih, K. Kavukcuoglu, D. Silver, A. Graves, I. Antonoglou, D. Wierstra, and M. Riedmiller, arXiv preprint arXiv:1312.5602 (2013).
- [24] V. Mnih, K. Kavukcuoglu, D. Silver, A. A. Rusu, J. Veness, M. G. Bellemare, A. Graves, M. Riedmiller, A. K. Fidjeland, G. Ostrovski, *et al.*, *Nature* **518**, 529 (2015).
- [25] M. G. Bellemare, Y. Naddaf, J. Veness, and M. Bowling, *Journal of Artificial Intelligence Research* **47**, 253 (2013).
- [26] V. Mnih, A. P. Badia, M. Mirza, A. Graves, T. Lillicrap, T. Harley, D. Silver, and K. Kavukcuoglu, in *International conference on machine learning* (2016) pp. 1928–1937.
- [27] Y. Tassa, Y. Doron, A. Muldal, T. Erez, Y. Li, D. d. L. Casas, D. Budden, A. Abdolmaleki, J. Merel, A. Lefrancq, *et al.*, arXiv preprint arXiv:1801.00690 (2018).
- [28] E. Todorov, T. Erez, and Y. Tassa, in *Intelligent Robots and Systems (IROS), 2012 IEEE/RSJ International Conference on* (IEEE, 2012) pp. 5026–5033.
- [29] M. L. Puterman, *Markov decision processes: discrete stochastic dynamic programming* (John Wiley & Sons, 2014).
- [30] A. Asperti, D. Cortesi, and F. Sovrano, arXiv preprint arXiv:1804.08685 (2018).
- [31] M. Riedmiller, in *European Conference on Machine Learning* (Springer, 2005) pp. 317–328.
- [32] M. Riedmiller, T. Gabel, R. Hafner, and S. Lange, *Autonomous Robots* **27**, 55 (2009).
- [33] J. Schulman, F. Wolski, P. Dhariwal, A. Radford, and O. Klimov, arXiv preprint arXiv:1707.06347 (2017).
- [34] F. P. Such, V. Madhavan, E. Conti, J. Lehman, K. O. Stanley, and J. Clune, arXiv preprint arXiv:1712.06567 (2017).
- [35] G. Brockman, V. Cheung, L. Pettersson, J. Schneider, J. Schulman, J. Tang, and W. Zaremba, arXiv preprint arXiv:1606.01540 (2016).
- [36] M. Kempka, M. Wydmuch, G. Runc, J. Toczek, and W. Jaśkowski, in *Computational Intelligence and Games (CIG), 2016 IEEE Conference on* (IEEE, 2016) pp. 1–8.
- [37] M. Wydmuch, M. Kempka, and W. Jaśkowski, arXiv preprint arXiv:1809.03470 (2018).
- [38] D. Silver, A. Huang, C. J. Maddison, A. Guez, L. Sifre, G. Van Den Driessche, J. Schrittwieser, I. Antonoglou, V. Panneershelvam, M. Lanctot, *et al.*, *nature* **529**, 484 (2016).
- [39] D. Silver, J. Schrittwieser, K. Simonyan, I. Antonoglou, A. Huang, A. Guez, T. Hubert, L. Baker, M. Lai, A. Bolton, *et al.*, *Nature* **550**, 354 (2017).
- [40] H. Touchette, *Physics Reports* **478**, 1 (2009).
- [41] J. P. Garrahan, R. L. Jack, V. Lecomte, E. Pitard, K. van Duijvendijk, and F. van Wijland, *Journal of Physics A: Mathematical and Theoretical* **42**, 075007 (2009).
- [42] F. Den Hollander, *Large Deviations*, Vol. 14 (American Mathematical Soc., 2008).
- [43] R. S. Ellis, *Entropy, large deviations, and statistical mechanics* (Springer, 2007).
- [44] C. Giardinà, J. Kurchan, and L. Peliti, *Physical Review Letters* **96**, 120603 (2006).
- [45] R. L. Jack and P. Sollich, *The European Physical Journal Special Topics* **224**, 2351 (2015).
- [46] U. Ray, G. K.-L. Chan, and D. T. Limmer, *Physical Review Letters* **120**, 210602 (2018).
- [47] M. C. Bañuls and J. P. Garrahan, arXiv preprint arXiv:1903.01570 (2019).
- [48] P. W. Glynn and D. L. Iglehart, *Management Science* **35**, 1367 (1989).
- [49] J. S. Sadowsky and J. A. Bucklew, *IEEE transactions on Information Theory* **36**, 579 (1990).
- [50] J. A. Bucklew, P. Ney, and J. S. Sadowsky, *Journal of Applied Probability* **27**, 44 (1990).
- [51] J. A. Bucklew, *Large deviation techniques in decision, simulation, and estimation* (Wiley New York, 1990).
- [52] S. Asmussen and P. W. Glynn, *Stochastic simulation: algorithms and analysis*, Vol. 57 (Springer Science & Business Media, 2007).
- [53] S. Juneja and P. Shahabuddin, *Handbooks in operations research and management science* **13**, 291 (2006).
- [54] J. Bucklew, *Introduction to rare event simulation* (Springer Science & Business Media, 2013).
- [55] D. Jacobson and S. Whitelam, arXiv preprint arXiv:1903.06098 (2019).
- [56] D. T. Gillespie, *The Journal of Physical Chemistry* **81**, 2340 (1977).
- [57] U. Seifert, *Physical Review Letters* **95**, 040602 (2005).
- [58] T. Speck, A. Engel, and U. Seifert, *Journal of Statistical Mechanics: Theory and Experiment* **2012**, P12001 (2012).
- [59] V. Lecomte, A. Imparato, and F. v. Wijland, *Progress of Theoretical Physics Supplement* **184**, 276 (2010).
- [60] É. Fodor, M. Guo, N. Gov, P. Visco, D. Weitz, and F. van Wijland, *EPL (EuroPhysics Letters)* **110**, 48005 (2015).
- [61] Y. Li and F. Cao, *European Journal of Operational Research* **224**, 333 (2013).
- [62] S. S. Singh, V. B. Tadić, and A. Doucet, *European Journal of Operational Research* **178**, 808 (2007).
- [63] The model's rates are $W_{12} = 3$, $W_{13} = 10$, $W_{14} = 9$,

- $W_{21} = 10, W_{23} = 1, W_{24} = 2, W_{31} = 6, W_{32} = 4, W_{34} = 1, W_{41} = 7, W_{42} = 9, \text{ and } W_{43} = 5.$
- [64] T. R. Gingrich, J. M. Horowitz, N. Perunov, and J. L. England, *Physical Review Letters* **116**, 120601 (2016).
- [65] P. Pietzonka, A. C. Barato, and U. Seifert, *Physical Review E* **93**, 052145 (2016).
- [66] J. P. Garrahan, *Physical Review E* **95**, 032134 (2017).
- [67] G. Fredrickson and H. C. Andersen, *Physical Review Letters* **53**, 1244 (1984).
- [68] J. P. Garrahan and D. Chandler, *Physical Review Letters* **89**, 035704 (2002).
- [69] J. P. Garrahan, R. L. Jack, V. Lecomte, E. Pitard, K. van Duijvendijk, and F. van Wijland, *Physical Review Letters* **98**, 195702 (2007).
- [70] A. Krizhevsky, I. Sutskever, and G. E. Hinton, in *Advances in neural information processing systems* (2012) pp. 1097–1105.
- [71] Y. LeCun, L. Bottou, Y. Bengio, P. Haffner, *et al.*, *Proceedings of the IEEE* **86**, 2278 (1998).
- [72] P. G. Bolhuis, D. Chandler, C. Dellago, and P. L. Geissler, *Annual Review of Physical Chemistry* **53**, 291 (2002).
- [73] K. Binder, in *Monte Carlo Methods in Statistical Physics* (Springer, 1986) pp. 1–45.
- [74] C. Maes and K. Netočný, *EPL (EuroPhysics Letters)* **82**, 30003 (2008).
- [75] L. Bertini, A. Faggionato, D. Gabrielli, *et al.*, in *Annales de l'Institut Henri Poincaré, Probabilités et Statistiques*, Vol. 51 (Institut Henri Poincaré, 2015) pp. 867–900.

S1. LARGE DEVIATIONS BY CHANGE OF MODEL

For completeness we present the derivation of Eq. (3) of the main text, which follows straightforwardly from the definition of the probability distribution. The derivation follows Ref. [55] with minor notational changes. For more on the ideas of dynamic importance sampling see e.g. Refs. [40, 48–54] and Ref. [16] (esp. Section 5).

Consider a continuous-time dynamics on a set of discrete states, defined by the master equation [73]

$$\partial_t P_x(t) = \sum_{y \neq x} W_{yx} P_y(t) - R_x P_x(t). \quad (\text{S1})$$

Here $P_x(t)$ is the probability that the system is in (micro)state x at time t , W_{xy} is the rate for passing from state x to state y , and $R_x = \sum_{y \neq x} W_{xy}$ is the escape rate from x . A standard way of simulating (S1) is as follows [56]: from state x , choose a new state y with probability

$$p_{xy} = \frac{W_{xy}}{R_x}, \quad (\text{S2})$$

and a time increment Δt from the distribution

$$p_x(\Delta t) = R_x e^{-R_x \Delta t}. \quad (\text{S3})$$

The dynamics defined by (S2) and (S3) generates a trajectory $\omega = x_0 \rightarrow x_1 \rightarrow \dots \rightarrow x_{N(\omega)}$ consisting of $N(\omega)$ jumps $x_n \rightarrow x_{n+1}$ and associated jump times Δt_n . Associated with an ensemble of trajectories of length T is the probability distribution

$$\rho_T(A) = \sum_{\omega} p(\omega) \delta(T) \delta(A) \quad (\text{S4})$$

of a time-extensive dynamical observable

$$A(\omega) = \sum_{n=0}^{N(\omega)-1} \alpha_{x_n x_{n+1}}. \quad (\text{S5})$$

In these expressions $\delta(X) \equiv \delta(X(\omega) - X)$ specifies a constraint on the trajectory, α_{xy} is the change of A upon moving from x to y , and $A(\omega)$ is the sum of these quantities over a single trajectory ω . We define $a(\omega) \equiv A(\omega)/T(\omega)$ as the time-intensive version of A . $T(\omega)$ is the elapsed time of trajectory ω , and $p(\omega)$ is the probability of a trajectory ω , proportional to a product of factors (S2) and (S3) for all jumps of the trajectory.

Fluctuations of a are quantified by $\rho_T(A)$, which for large T often adopts a large-deviation form [40, 42]

$$\rho_T(A) \approx e^{-TJ(a)}. \quad (\text{S6})$$

Direct evaluation of (S4) using the dynamics (S2) and (S3) leads to good sampling of $J(a)$ near the typical value a_0 , where $J(a_0) = 0$, and poor sampling elsewhere. To overcome this problem we can introduce a reference dynamics

$$\tilde{p}_{xy} = \frac{\tilde{W}_{xy}}{\tilde{R}_x}, \quad (\text{S7})$$

and

$$\tilde{p}_x(\Delta t) = \tilde{R}_x e^{-\tilde{R}_x \Delta t}, \quad (\text{S8})$$

in which \tilde{W}_{xy} is a modified version of the rate of the original model, and $\tilde{R}_x \equiv \sum_y \tilde{W}_{xy}$. Let $\tilde{p}(\omega)$ be the trajectory weight of the reference dynamics, proportional to a product of factors (S7) and (S8) for all jumps of the trajectory. We write

$$\langle \cdot \rangle^a \equiv \sum_{\omega} p(\omega) (\cdot) \delta(T) \delta(aT) \quad (\text{S9})$$

and

$$\langle \cdot \rangle_{\text{ref}}^a \equiv \sum_{\omega} \tilde{p}(\omega) (\cdot) \delta(T) \delta(aT) \quad (\text{S10})$$

for the ensemble averages over trajectories (having length T and observable $A = aT$) of the original and reference models, respectively. We can then write (S4) as

$$\rho_T(A) = \langle 1 \rangle^a = \langle e^{Tq(\omega)} \rangle_{\text{ref}}^a \quad (\text{S11})$$

$$= e^{T\langle q(\omega) \rangle_{\text{ref}}^a} \langle e^{T\delta q(\omega)} \rangle_{\text{ref}}^a. \quad (\text{S12})$$

Here $e^{Tq(\omega)} = p(\omega)/\tilde{p}(\omega)$ is the reweighting factor (also known as the likelihood ratio or Radon-Nikodym derivative [16, 54]). We have

$$q(\omega) = T^{-1} \ln \frac{p(\omega)}{\tilde{p}(\omega)} = -T^{-1} \sum_{n=0}^{N-1} q_{x_n x_{n+1}}, \quad (\text{S13})$$

where

$$q_{x_n x_{n+1}} = \ln \frac{W_{x_n x_{n+1}}}{\tilde{W}_{x_n x_{n+1}}} - \tilde{\Delta} t_n (R_{x_n} - \tilde{R}_{x_n}). \quad (\text{S14})$$

Here $\tilde{\Delta} t_n = -\ln \eta / \tilde{R}_{x_n}$ is the jump time of the reference model (η is a random number uniformly distributed on $(0, 1]$). In (S12) the quantity $\delta q(\omega) \equiv q(\omega) - \langle q(\omega) \rangle_{\text{ref}}^a$.

Taking logarithms of (S12) and the large- T limit gives us

$$J(\tilde{a}_0) = J_0(\tilde{a}_0) + J_1(\tilde{a}_0), \quad (\text{S15})$$

where

$$J_0(\tilde{a}_0) = -\langle q(\omega) \rangle_{\text{ref}}^{\tilde{a}_0} \quad (\text{S16})$$

and

$$J_1(\tilde{a}_0) = -\frac{1}{T} \ln \langle e^{T\delta q(\omega)} \rangle_{\text{ref}}^{\tilde{a}_0}. \quad (\text{S17})$$

In these expressions \tilde{a}_0 is the typical value of a for the reference model. The term (S16) is by Jensen's inequality an upper bound on the piece of the rate function $J(a)$ at the point $a = \tilde{a}_0$, i.e

$$J(\tilde{a}_0) \leq J_0(\tilde{a}_0). \quad (\text{S18})$$

The bound can be determined by computing the values of (S5) and (S13) for a suitably long reference-model trajectory. The correction term (S17) can be determined by sampling values of q for the reference model, provided that the typical dynamics of the reference model is close enough to the desired conditioned dynamics of the original model [55].

If the reference model's typical dynamics is similar to the conditioned rare dynamics of the original model (something we generally do not know in advance), then the bound $J_0(\tilde{a}_0)$ will be tight, and if it is tight enough the exact value of $J(\tilde{a}_0)$ can be calculated by sampling the (slightly) atypical behavior of the reference model [55]. The optimal reference model, called the driven or auxiliary process [16, 40, 45, 54], is one for which the bound is exact, meaning that its typical behavior is equivalent to the conditioned rare behavior of the original model. In the main text we show that evolutionary reinforcement learning can generate optimal or near-optimal reference models, for which the correction term is negligible.

S2. 4-STATE MODEL EVOLUTIONARY PROCEDURE

The evolutionary procedure used to make Fig. 1 of the main text is as follows. We start by running a trajectory

of the reference model (of $N = 10^4$ events) and recording the typical value of the observable and bound, the long-time limits of (1) and (3), respectively. Initially the reference model is the original model, $\tilde{W}_{xy} = W_{xy}$, and so $a = a_0$ and $J_0 = 0$.

To perform an evolutionary step we create a mutant model whose rates are

$$\hat{W}_{xy} = e^{\epsilon(\eta_{xy}-1/2)} \tilde{W}_{xy}. \quad (\text{S19})$$

Here ϵ is an evolutionary rate and η_{xy} is a uniformly distributed random number on $(0, 1]$. With this new set of rates we run a new trajectory and compute the new values of a and J_0 , called \hat{a} and \hat{J}_0 , respectively. If our selection criteria are fulfilled (see below) then we accept the mutation, and set $\tilde{W}_{xy} = \hat{W}_{xy}$, $a = \hat{a}$, and $J_0 = \hat{J}_0$ (the mutant model becomes the new reference model); if not, we retain the current reference model.

We imposed two types of selection criteria. For the first, called a -evolution, we accepted the mutation if \hat{a} is closer than a to a specified target value a^* , i.e. if

$$|\hat{a} - a^*| < |a - a^*|. \quad (\text{S20})$$

For the second, called J -evolution, we accept the mutation if \hat{J}_0 is smaller than J_0 and if \hat{a} lies within a tolerance $\delta = 0.1$ of a specified pinning value a^\dagger , i.e. if

$$\hat{J}_0 < J_0 \quad \text{and} \quad |\hat{a} - a^\dagger| < \delta. \quad (\text{S21})$$

The process of a -evolution leads to reference models able to generate values of a far from a_0 , while J -evolution leads to reference models that generate values of a in a manner as close as possible to the original model.

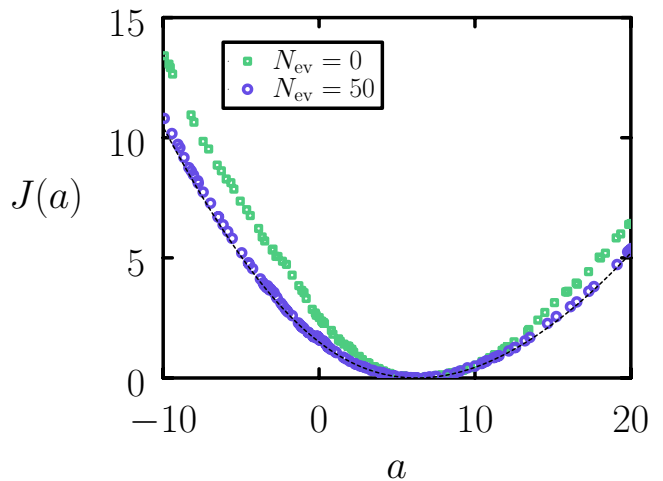


FIG. S1. Similar to Fig. 1 of the main text, using an evolutionary scheme in which we alternate 5 steps of a -evolution with N_{ev} steps of J -evolution, for different target values of the observable a . The results reported in Fig. 1 were produced from the set $N_{\text{ev}} = 50$ using an additional 10^5 steps of J -evolution once the desired value of a was achieved.

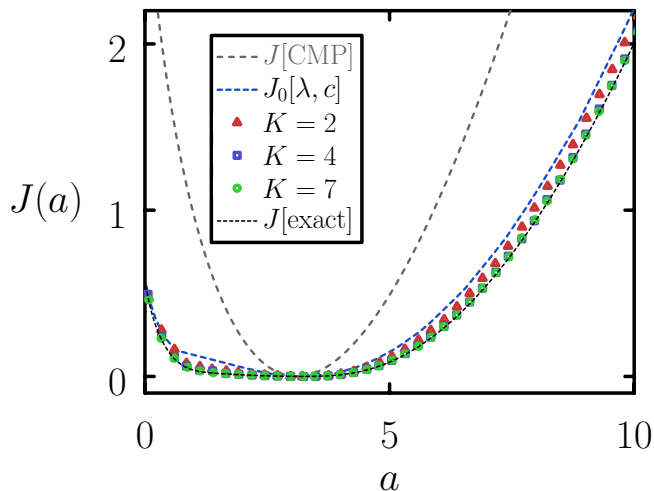


FIG. S2. (a) Similar to Fig. 3(a) of the main text, showing results for neural-network spin filters up to order $K = 2, 4, 7$. For $K \gtrsim 4$ the bound is numerically close to the exact answer. Also shown is the CMP universal activity bound [66] (gray), which results from the typical dynamics of a reference model whose rates are uniform multiples of those of the original model, and the (c, λ) bound of Ref. [55] (blue). The latter is essentially equivalent to the case $K = 1$.

To produce Fig. 1 we alternated 5 steps of a -evolution, using an evolutionary rate of $\epsilon = 0.1$, with 50 steps of J -evolution, using an evolutionary rate of $\epsilon = 0.05$. During J -evolution we chose the pinning value a^\dagger to be the last value of a produced by the preceding phase of a -evolution. Upon reaching a specified value a^* we carried out an additional 10^5 steps of J evolution (with $a^\dagger = a^*$), again using $\epsilon = 0.05$. We carried out 100 independent simulations, each with a different target value a^* .

Fig. 1 shows results obtained in this way; Fig. S1 shows results obtained using fewer steps of J -evolution.

S3. FA MODEL EVOLUTIONARY PROCEDURE

Each proposed evolutionary move consisted of a shift of each weight $w \in \{w_0, w_1, w_k^\alpha\}$ of the reference model (5) by independent Gaussian-distributed random numbers of zero mean and variance $\sigma^2 = 10^{-4}$:

$$w \rightarrow w + \mathcal{N}(0, \sigma^2). \quad (\text{S22})$$

We ran trajectories for $N = 10^5$ events, and recorded the values of (1) and (3) after each proposed trajectory. We did a -evolution on the parameters w_0 and w_1 until a specified value a^* was reached. This procedure was as described for the 4-state model, with the additional restriction that the new bound must be not more than a value $\epsilon = 0.2$ larger than the current bound. That is, the

proposed set of weights was accepted if

$$|\hat{a} - a^*| < |a - a^*| \quad \text{and} \quad \hat{a} < a + \epsilon. \quad (\text{S23})$$

We then did J -evolution using a tolerance of $\delta = 0.02$ [see Eq. (S21)], for 3×10^4 proposed trajectories, with higher-order spin filters applied. We ran 50 simulations, each with a different target value of a .

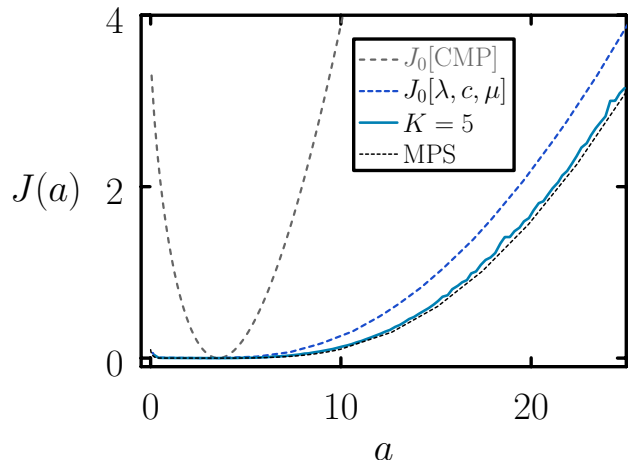


FIG. S3. (a) Similar to Fig. 3(a) of the main text, but using the FA model of Ref. [47] ($L = 100, c = 0.1$). We show the CMP universal activity bound [66] (gray), the three-parameter bound of Ref. [55] (blue), the results of evolutionary learning (blue-green) using the network shown in Fig. 2 of the main text with $K = 5$ (10 free parameters), and the exact answer obtained using matrix product states [47] (black).

In Fig. S2 we reproduce some of the results shown in Fig. 3(a) of the main text, together with results obtained for different values of K .

We also tested the method on the 100-site FA model of Ref. [47], whose state space is large enough that state-of-the-art methods are needed to compute its large-deviation rate function. We addressed this model using evolutionary learning on the network shown in Fig. 2 (with $K = 5$). We ran 100 different simulations with target values of a between 0.1 and 25 (the typical value of the original model is approximately 3.5). We turned on all filters from the start, and used trajectories of $N = 3 \times 10^5$ events. We used a -evolution to generate the desired values of a , and then did J -evolution for 10^4 proposed trajectories. Results are shown in Fig. S3: the bound produced is inexact, but close enough to the exact answer to suggest that modifications of the present scheme can converge to this answer (we note that the model of Ref. [47] uses open boundaries, and the network of Fig. 2 is designed with periodic boundaries in mind).

S4. THE CMP UNIVERSAL ACTIVITY BOUND

The Conway-Maxwell-Poisson (CMP) formula

$$J[\text{CMP}] = \frac{k_0}{a_0} \left(a \ln \frac{a}{a_0} + a_0 - a \right), \quad (\text{S24})$$

gives a bound on the large-deviation rate function $J(a)$ for any non-decreasing counting observable a ; here a_0 is the typical value of the observable, and k_0 is the typical dynamical activity k (the total number of configuration changes per unit time). Eq. (S24) was derived in Ref. [66] from Level 2.5 of large deviations [74, 75], and we have used this form in Fig. 3, Fig. S2, and Fig. S3 (for the case $a = k$).

We note that the CMP formula can also be straightforwardly derived from the bound (3). Let a_0 and k_0 be the typical activities produced by an original model W_{xy} . Then a reference model $\tilde{W}_{xy} = \gamma W_{xy}$, whose rates are uniformly rescaled versions of those of the original model, will produce typical activities γa_0 and γk_0 (a uniform rescaling of rates does not affect the choice of new state,

i.e. $\tilde{W}_{xy}/\tilde{R}_x = W_{xy}/R_x$, and so the reference model will visit the same set of states as the original model, just faster or slower).

In (3) we can replace the fluctuating jump time $\tilde{\Delta}t_n$ with its mean $1/\tilde{R}_{x_n}$, valid in the long-time, steady-state limit, and replace \tilde{R}_{x_n} with γR_{x_n} , giving

$$\begin{aligned} J_0 &= T^{-1} \sum_{n=0}^{N-1} \left(\ln \gamma + \frac{1-\gamma}{\gamma} \right) \\ &= k \left(\ln \frac{a}{a_0} + \frac{a_0 - a}{a} \right) \\ &= \frac{k}{a} \left(a \ln \frac{a}{a_0} + a_0 - a \right) \\ &= \frac{k_0}{a_0} \left(a \ln \frac{a}{a_0} + a_0 - a \right), \end{aligned} \quad (\text{S25})$$

which is Eq. (S24). In (S25) we have written $k = N/T$ for the total number of configuration changes per unit time, and have used the relations $k = \gamma k_0$ and $a = \gamma a_0$.